Research Square

Preprints are preliminary reports that have not undergone peer review.
They should not be considered conclusive, used to inform clinical practice,
or referenced by the media as validated information.

Digital Restoration of Near Axially Symmetric Ceramics via Geometric Constraints and Surface Priors

Wang Yi

wangyisj@sust.edu.cn

Shaanxi University of Science and Technology

Si Ziqing

Shaanxi University of Science and Technology

Zhu Jianfeng

Shaanxi University of Science and Technology

Wang Tian

Shaanxi University of Science and Technology

Quan Min

Shaanxi Academy of Cultural Relics Conservation (Shaanxi Identification Center of Cultural Relics)

Zhou Yang

Shaanxi Academy of Cultural Relics Conservation (Shaanxi Identification Center of Cultural Relics)

Wang Weiwei

Shaanxi University of Science and Technology

Chen Jian

Shaanxi University of Science and Technology

Yang Xiaoyan

Shaanxi University of Science and Technology

Article

Keywords:

Posted Date: November 26th, 2026

DOI: https://doi.org/10.21203/rs.3.rs-11541482/v1

License: This work is licensed under a Creative Commons Attribution 4.0 International License.
Read Full License

Additional Declarations: No competing interests reported.

Digital Restoration of Near Axially Symmetric Ceramics via Geometric Constraints and Surface Priors

Wang Yi [1,3] (Corresponding Author), Si Ziqing [1] , Zhu Jianfeng [2,3] , Wang Tian [2,3] , Quan Min [4] , Zhou Yang [4] , Wang Weiwei [1] , Chen Jian [1] , Yang Xiaoyan [1]

(1. School of Design and Art, Shaanxi University of Science and Technology, Xi'an, Shaanxi 710021;2. School of Materials Science and Engineering, Shaanxi University of Science and Technology, Xi'an, Shaanxi 710021; 3. Key Laboratory of Materials and Technologies for the Conservation of Underground Cultural Relics (Shaanxi University of Science and Technology), Xi'an, Shaanxi 710021; 4. Shaanxi Academy of Cultural Relics Conservation (Shaanxi Identification Center of Cultural Relics), Xi'an, Shaanxi 710075)

Abstract: Digital restoration of ancient ceramics faces the challenge of concurrent geometric damage and missing surface information; existing methods struggle to balance three-dimensional structural integrity with surface continuity. This paper focuses on near-axially symmetric ceramics and combines 3D scan models with grayscale ceramic images to develop a two-stage digital restoration method that integrates geometric constraints with surface priors. The AdaPoinTr geometric reconstruction algorithm was optimized using damage boundaries, sound cross-section contours, and local symmetry constraints, while smooth glaze shading and the relief patterns of incised decorations were used to construct surface prior models. Case studies demonstrate that the state of preservation of the rim and key cross-sections helps explain differences in the reconstruction results; statistical reconstruction and surface visualization, respectively, illustrate the expressive capabilities and application performance of the classification-based priors. This study provides a workflow reference for constructing geometric patches and generating surfaces for nearly axisymmetric ceramic objects.

1. Introduction

Ancient ceramics constitute an important category of cultural heritage within archaeological sites and museum collections. Long-term exposure to burial environments, mechanical stress, and human factors often results in issues such as physical breakage, surface erosion, and the loss of decorative details. Traditional physical restoration primarily relies on inferring missing forms based on surviving structures, comparable artifacts, and restoration experience; however, this approach carries a degree of subjectivity when complete references are lacking. Non-contact 3D scanning and digital modeling technologies offer new avenues for research on damaged ceramics, enabling structural analysis and virtual restoration without interfering with the artifact itself.

As digital technology has evolved from shape capture to the inference of missing information, geometric rules and data-driven methods have gradually been applied to the digital reconstruction of archaeological artifacts. Núñez-Andrés et al.[1] used photogrammetric data and geometric features to virtually reconstruct archaeological pottery; Lamb et al. [2]

constructed a paired dataset of damaged objects and intact models, providing a foundation for 3D reconstruction and quantitative evaluation. However, it is often difficult to obtain complete 3D models of ancient ceramics before breakage, and variations in artifact forms and preservation conditions make constructing geometric references and evaluating restoration with limited samples challenging.

In the field of 3D geometric reconstruction, deep learning methods have improved the ability to infer the morphology of complex damaged regions by learning shape distribution patterns. Xu et al.[3] proposed a Terracotta Army reconstruction network based on conditional point diffusion, while Yu et al. [4] introduced AdaPoinTr, which establishes a correlation between the remaining point cloud and the missing morphology through an adaptive geometry-aware Transformer.ProxyFormer [5], AnchorFormer [6], and PointAttN [7] optimize completion performance by addressing missing feature representation, anchor modeling, and attention mechanisms, respectively. SDS-Complete [8] and DAPoinTr [9] alleviate the issues of insufficient domain-specific data and domain-specific scanning differences by leveraging pre-trained generative priors and cross-domain adaptation. However, general-purpose completion methods still rely heavily on the shape distribution of the training data, making it difficult to fully meet the specific requirements of ceramic artifacts, such as boundary matching, contour preservation, and surface continuity.

Wheel-thrown ceramics typically exhibit near-axial symmetry, and their main form can be described by a central axis, longitudinal contour, and cross-sections of the inner and outer walls. Wu et al. [10] improved point cloud completion results by introducing structural priors, while Wang Zhengrong et al.[11] explored the application of diffusion models in 3D void filling for cultural relics, providing a reference for combining structural constraints with intelligent completion. However, in actual ceramic artifacts, rim deformations, handle components, and local decorations may result in asymmetric structures, while large-area damage can lead to insufficient cross-sectional information. Uniform, strong axisymmetric constraints tend to obscure the artifact's inherent local features; therefore, it is necessary to apply adaptive geometric constraints to candidate reconstruction results by integrating structural credibility, primary damage boundaries, and sound cross-sectional contours.

In addition to 3D shape reconstruction, the restoration of surface appearance information is also a critical aspect of the digital restoration of ceramics. In recent years, Zhang [12] utilized LoRA and Stable Diffusion to restore patterns on Yangshao painted pottery; Kang et al. [13] employed an improved diffusion model to restore patterns on Jingdezhen export porcelain; and Liao et al.[14] combined adversarial learning with inverse diffusion to predict missing regions in images of ancient ceramics.ControlNet [15], Custom Diffusion [16] BrushNet [17], and PowerPaint [18] have each enhanced image restoration capabilities in the areas of spatial condition control, few-shot adaptation, and local generation, respectively. To address the complex damage in cultural heritage images, Wu Meng et al. [19], Hu et al. [20], Li et al. [21], Ding et al. [22], and Tian Bin et al. [23] improved mural restoration results through contextual inference, diffusion guidance, and structural constraints. However, existing methods primarily focus on 2D pattern generation [24] and still lack targeted priors for the low-frequency light-and-shadow variations in smooth ceramics and the local concave-convex textures in engraved ceramics.

Existing 3D geometric completion and 2D surface restoration are often treated as independent tasks; however, ceramic patterns and engraved features are closely related to surface curvature, depth, and normal information, and relying solely on 2D image context can easily lead to inconsistencies between the generated content and the spatial form. Cao et al. [25] proposed TexFusion, which improves 3D texture consistency through multi-view diffusion generation; Zeng et al.[26] proposed Paint3D, which combines depth conditions with texture-space restoration, offering a new approach to the collaborative generation of geometric and surface information. However, general-purpose methods still struggle to fully adapt to the specific geometric structures and local decorative features of ancient ceramics, and historical patterns that are completely missing often lack verifiable ground truth. Therefore, it is necessary to combine the actual geometric substrate with the remaining surface information to establish type-specific surface priors, thereby improving the visual continuity of patches and controlling restoration uncertainty.

Based on the above issues, this paper constructs a two-stage digital restoration workflow—geometric constraints and surface priors—tailored for nearly axially symmetric ceramics. In the geometric stage, the pre-trained AdaPoinTr model is used to generate candidate restoration results, and the patch shape is adjusted based on the primary defect boundary, the intact cross-section contour, and local symmetry weights. In the surface stage, statistical modeling is performed separately for the low-frequency luminance variations of smooth ceramics and the high-frequency residuals and gradient features of incised ceramics; the priors are then applied to the geometric patches via UV mapping. The study constructed four levels of artificial defects from three scanned artifacts to analyze geometric reconstruction performance under varying residual structural conditions. Additionally, the expression and application of categorized priors were examined using holdout-sample reconstruction and 3D visualization. This paper focuses on the roles of the artifact's intrinsic geometric evidence and surface statistical priors within the same restoration workflow, as well as the method's applicability under conditions of critical structural loss.

2. Methodology

This chapter introduces a two-stage digital restoration method for near-axially symmetric ceramic artifacts that combines geometric constraints and surface priors. The method consists of four parts: data construction and preprocessing, geometric constraint-based reconstruction, learning of surface priors, and restoration evaluation. The overall technical framework is shown in Figure 1.

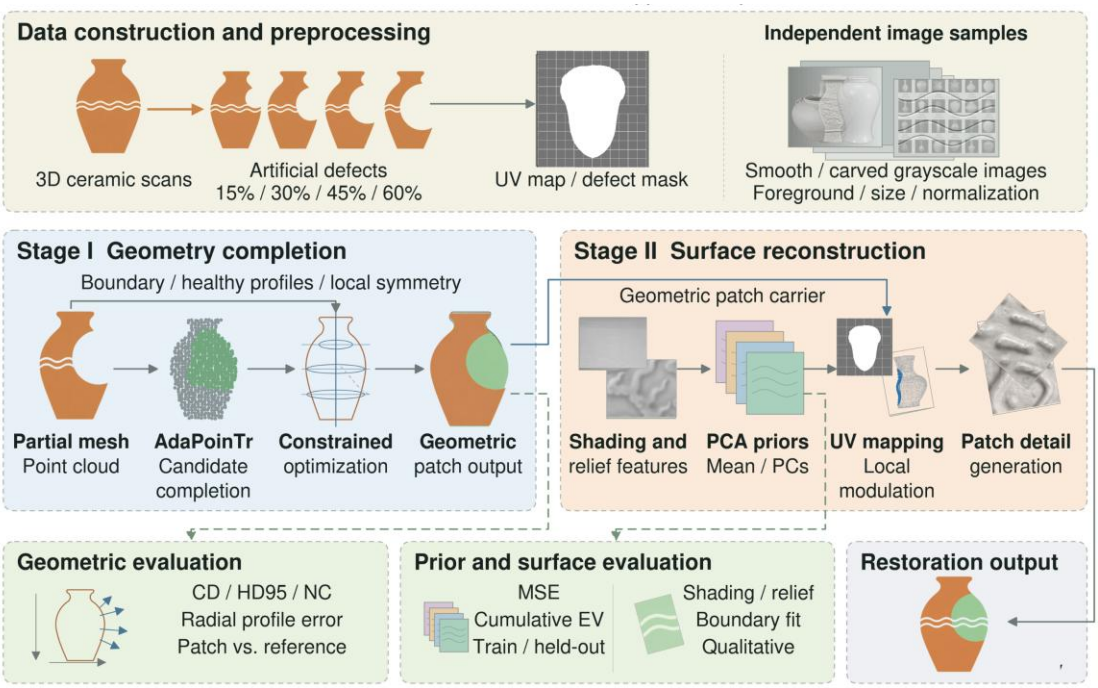

Fig. 1. Technical approach for the restoration method (Source: Drawn by the author.)

2.1 Data Construction and Preprocessing

The data used in this study consist of three components: 3D-scanned ceramic models, smooth ceramic grayscale images, and incised ceramic grayscale images, which are used for geometric reconstruction, low-frequency lighting and shading prior learning, and local surface texture modeling, respectively. Among these, the 3D scan models serve as a reference for simulating artifact damage and conducting geometric evaluation; the smooth ceramic images primarily characterize the continuous light-dark variations on the glazed surface; and the incised ceramic images are used to extract local grayscale gradient features formed by grooves, raised ridges, and decorative lines. To balance morphological diversity with structural representativeness, ceramic and glazed ceramic artifacts with varying body contours, rim structures, and surface decorative features were selected as 3D research samples. Figure 2 shows photographs of three representative artifacts and their 3D scan models, presenting the overall form and local structures of the artifacts from front, side, and top views, respectively.

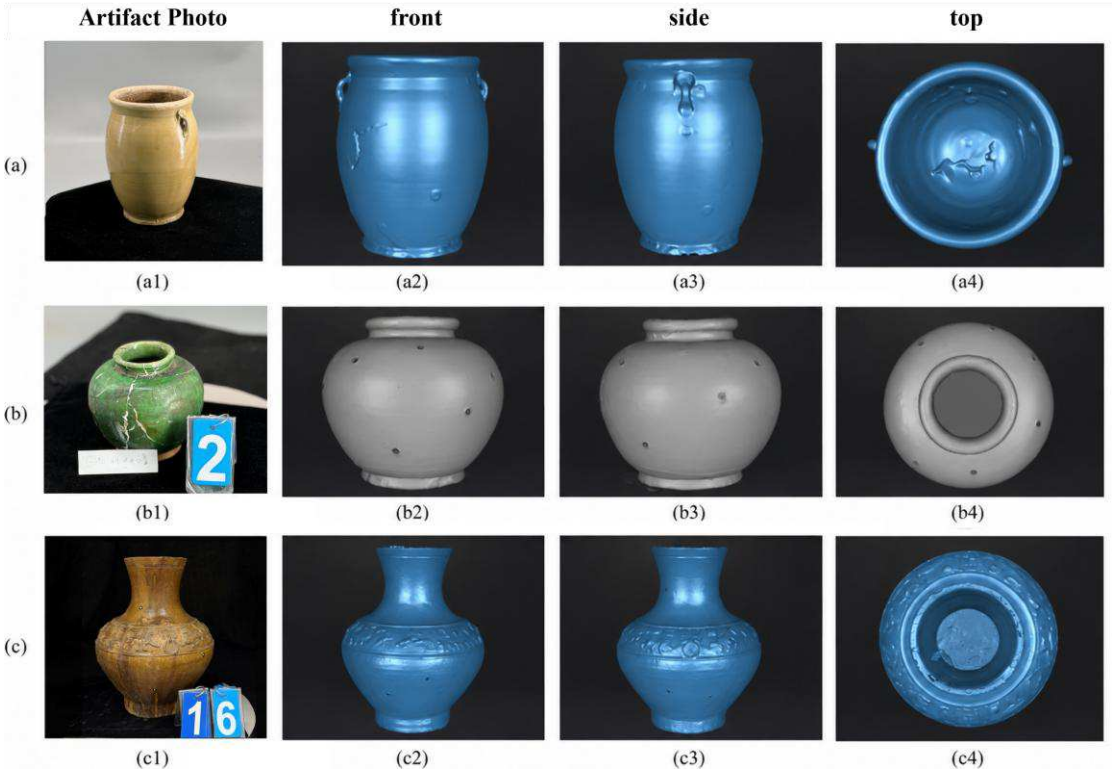

Figure 2. Examples of scanned ceramic artifacts and 3D models (Source: taken by the author and rendered from 3D scans)

Since actual damaged artifacts typically lack complete geometric ground truth, this study constructs artificial damage samples from complete scan models to establish a correspondence between damaged input data and the complete reference ground truth [27]. First, the original triangular mesh undergoes topological inspection, correction of anomalous faces, and coordinate normalization to align the surface normals with the artifact's main axis. Subsequently, to observe geometric reconstruction performance under different conditions of remaining structure, this study established two types of progressive loss patterns: Artifact 1 and Artifact 2, which employed axial progressive loss from the rim toward the body (15%, 30%, 45%, 60%), while Artifact 3 featured a large-area lateral loss spanning the neck, body, and incised band. These configurations were used to compare reconstruction performance across cases and to analyze differences in relation to defect location and the preservation status of key structural features. After sampling, each defect mesh was converted into an AdaPoinTr input point cloud, while the original geometry of the intact regions and the complete reference mesh were retained for subsequent surface reconstruction and error evaluation [28]. The defect ratio ρ is defined as:

$$\rho = \frac{A_{\text{miss}}}{A_{\text{full}}} \times 100\%$$

where A_{miss} and A_{full} represent the surface areas of the defect region and the complete model, respectively; the complete model serves as the geometric ground truth for all sampling levels.

To establish a correspondence between the 3D defect and the 2D surface information, a

conformal UV parameterization method is used to unfold the reference mesh into a 2D texture space. A local mapping between 3D surface points and UV coordinates is established through triangle indexing and centroid interpolation [29], and a binary defect mask is generated based on the removed triangles:

$$M(u,v) = \begin{cases} 1, & (u,v) \in \Omega_{\text{miss}} \\ 0, & (u,v) \in \Omega_{\text{valid}} \end{cases}$$

In this context, the damaged region and the intact region are denoted as Ω_{miss} and Ω_{valid} , respectively. The mask is used to define the scope of subsequent apparent reconstruction, thereby preventing modifications to the original surviving surface; for genuinely damaged artifacts, corresponding texture mapping is established after the geometric patch is constructed. Figure 3 illustrates the 3D morphology of the third artifact at different damage levels, along with the corresponding UV unfolding and mask projection processes.

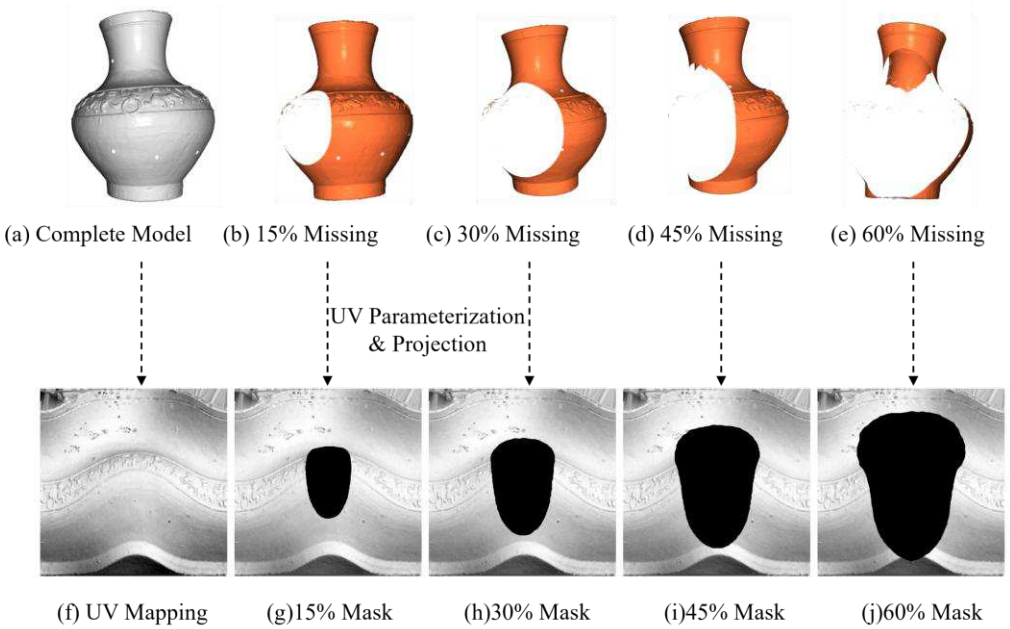

Fig. 3. Multi-level defect construction, 2D UV unfolding, and mask projection of a ceramic 3D model. (a) Complete 3D model; (b)–(e) 3D surface changes at different defect levels (15%, 30%, 45%, and 60%); (f)–(j) Corresponding 2D UV maps and projected mask areas. (Source: Author's experiments and 3D visualization generation.)

The 2D surface data were sourced from the team's self-built image database of ceramic cultural heritage, focusing on images of vases, jars, and other ceramics of similar forms. Based on surface characteristics, the data were classified into two grayscale datasets: smooth ceramics (553 pieces) and engraved ceramics (291 pieces). The former was used to learn low-frequency brightness variations on continuous surfaces, while the latter was used to extract high-frequency relief features—such as incised lines, ripples, and shallow relief areas. During the preprocessing stage, valid surface regions were obtained through foreground extraction and background removal. Double cubic interpolation was used to standardize the images to 512×512 pixels. Gray-scale normalization and histogram matching were combined to mitigate variations in imaging conditions while preserving the continuous gray-scale gradients in

smooth areas and the local gradient features in engraved areas, thereby providing standardized samples for subsequent appearance-prior learning.

2.2 Geometric Constraint-Based Reconstruction

To address incomplete geometric information resulting from damage to ancient ceramic artifacts, this paper employs the pre-trained AdaPoinTr as the initial point cloud completion network. This model establishes a correlation between local structure and overall morphology through adaptive query generation and a geometry-aware Transformer [4], thereby generating candidate geometries for the missing regions. However, general-purpose reconstruction networks rely on the shape distribution in the training data; when the target artifact differs from the training samples, issues such as contour offset and discontinuities in surface connections are likely to occur [30]. Therefore, while retaining the core network structure of AdaPoinTr, this study introduces the primary damage boundary, the contour of the intact cross-section, and local symmetry confidence to impose geometric constraints on the candidate reconstruction results [10].

First, a set of boundary points is extracted based on the open edges of the original triangular mesh. By combining connected component analysis, boundary scale, and spatial position, the primary defect regions are identified, and minute voids caused by scan noise are excluded. The primary defect boundary is used to define the patch generation range, while the original vertex coordinates and local normal information of the healthy regions are retained to prevent the reconstruction process from altering the actual existing surface.

Second, object-specific morphological priors are extracted from the healthy regions. For axially symmetric ceramic bodies, the central axis is estimated by fitting circular cross-sections, and horizontal cross-sections are extracted along the axis to establish radial contours for both the inner and outer walls. For rolled edges, rim edges, and double-walled structures, the relationship between the curvature of the inner and outer walls and the variation in adjacent cross-sections is further analyzed to avoid directly substituting the defect region with an ideal rotational surface. At the same time, local exclusion zones are established in the intact regions; the reliability of the geometric prior is verified by testing the deviation between the measured contour and the interpolated predicted contour, and candidate contours constrained by the boundaries are constructed. The process of locating the main missing area boundary and constructing local geometric priors is shown in Figure 4.

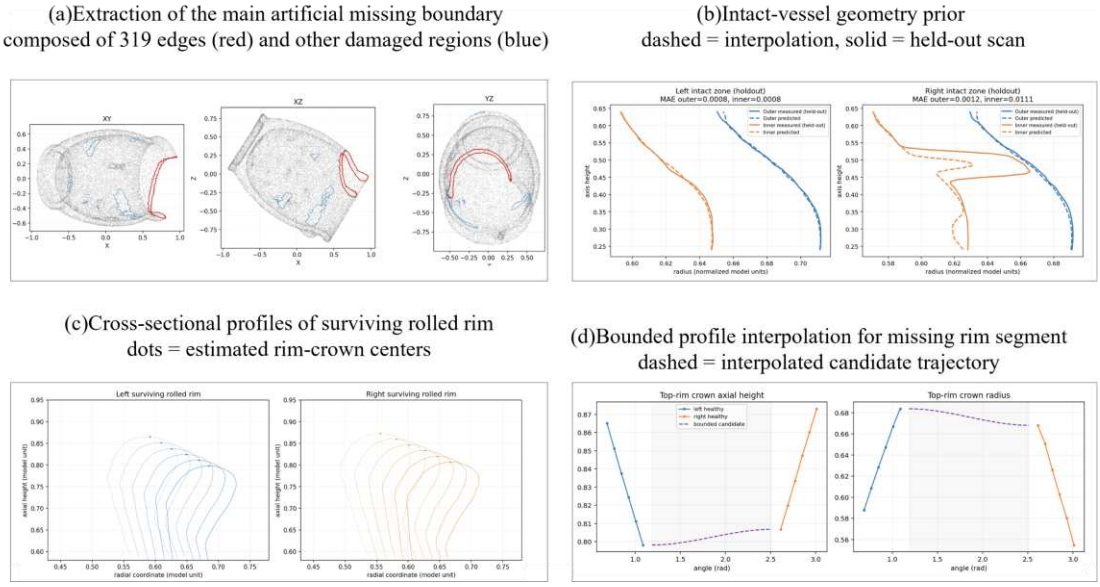

Fig. 4 Main missing area localization and local geometric prior construction for ancient ceramics.

(a) Manual identification of missing boundaries; (b) Geometric priors of the inner and outer walls and verification of the healthy area reservation; (c) Cross-section extraction of the surviving rolled rim; (d) Morphology prediction of the bounded rolled rim. (Source: Drawn by the author)

To avoid the strict assumption of axial symmetry from undermining the object's inherent asymmetrical characteristics, this paper constructs a local symmetry credibility based on the radial dispersion of the intact cross-section. For a horizontal cross-section with axial height (z), the average radial distance$\left(\bar{r}(z)\right)$ and standard deviation$\left(\sigma_r(z)\right)$ of the sampling points are calculated, and the normalized radial irregularity is defined as:

$$q(z) = \frac{\sigma_r(z)}{\bar{r}(z) + \varepsilon}$$

Symmetry credibility is further defined using a monotonically decreasing function:

$$w_{\mathrm{sym}}(z) = \phi\left(q(z)\right)$$

where(ε) is a numerically stable term, and$\left(\phi(\cdot)\right)$ is a monotonically decreasing mapping function. When the cross-section profile is relatively regular, the symmetry credibility is high; when local features such as ears, handles, or obvious asymmetrical decorations are present, the constraint weight decreases with increasing radial dispersion. For cross-sections with insufficient sampling or scanning anomalies, their weight in the optimization process is reduced to prevent unreliable prior information from interfering with the interpolation results.

Building on this, using the candidate patches generated by AdaPoinTr as an initial reference, and combining point set consistency, boundary normal continuity, local symmetry, and cross-section contour constraints, a joint geometric optimization objective is established:

$$L_{\text{geo}} = \lambda_{\text{cd}} L_{\text{CD}} + \lambda_n L_{\text{normal}} + \lambda_{\text{sym}} L_{\text{sym}} + \lambda_{\text{profile}} L_{\text{profile}}$$

where(L_{CD}) is used to constrain the point set consistency of candidate patches,(L_{normal}) controls the boundary normal continuity between the patch and the surviving surface,(L_{sym}) limits the radial deviation in near-axisymmetric regions based on local credibility, and(L_{profile}) constrains the deviation between the patch and the reference contour of the healthy cross-section. The weights(λ) are used to adjust the contribution of different constraints. During the optimization process, the original healthy region is fixed, and only the local geometry of the defect patch is adjusted to balance the object's overall contour with its local structural features.

To examine the spatial distribution of candidate patches under different defect conditions, this paper presents the residual point cloud and candidate smooth outer-wall patches from three orthogonal projection angles—XY, XZ, and YZ—for four levels of artificial defect samples (15%, 30%, 45%, and 60%), as shown in Figure 5. This figure is used to examine the spatial coverage of the patches, the correspondence of their contours, and the locations of boundary connections, providing a foundation for the subsequent evaluation of geometric restoration results.

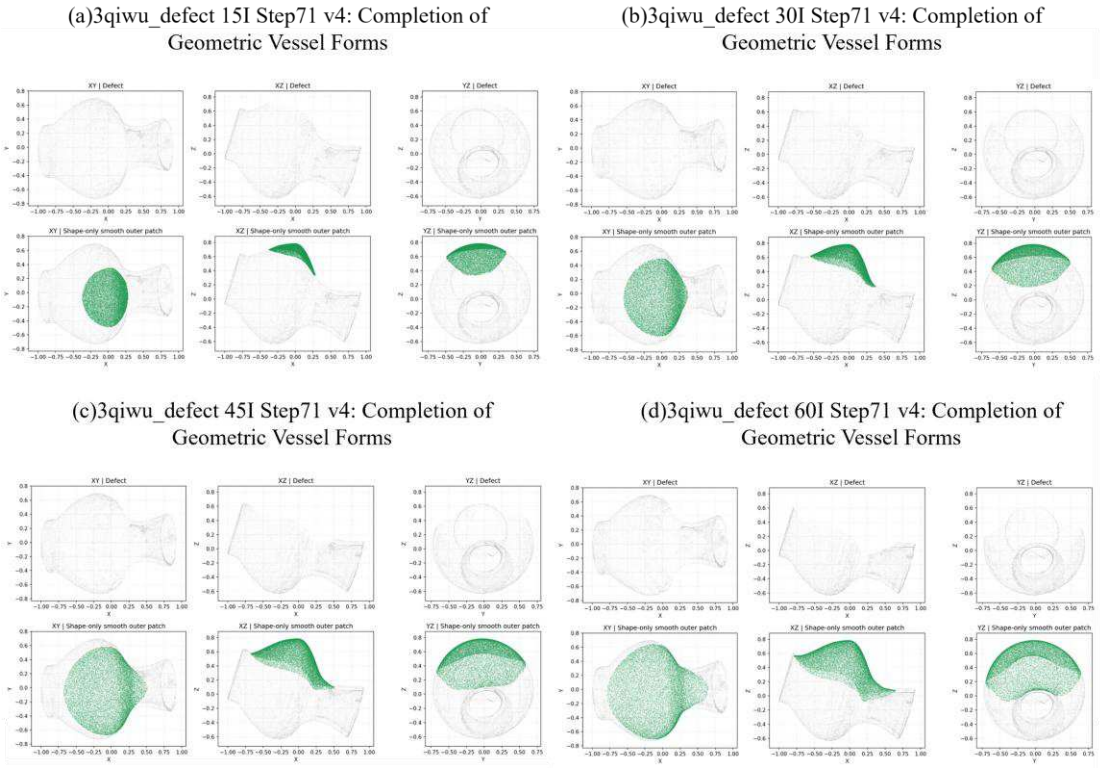

Figure 5 Candidate results of missing surface reconstruction for ceramic artifacts under different missing proportions. (a) 15% missing; (b) 30% missing; (c) 45% missing; (d) 60% missing. (Source: Drawn by the author.)

2.3 Prior Surface Modeling

The restoration of ancient ceramic surfaces involves not only the geometric

reconstruction of damaged areas but also the consideration of visual information such as variations in glaze brightness, incised patterns, and local surface irregularities. Existing image restoration methods primarily rely on texture matching, feature transfer, or generative models to reconstruct missing content; however, visual continuity in two-dimensional images does not necessarily correspond to spatial consistency on three-dimensional surfaces[31][32]. Therefore, building upon geometric completion, this paper constructs grayscale appearance statistical priors separately for smooth and incised ceramics, and combines them with features from the damage neighborhood for local modulation to harmonize the visual relationship between the patch's appearance and that of the original artifact.

To prevent the appearance reconstruction from altering the geometric information of the original scanned area, the generated patch is first extracted as an independent surface unit based on the primary defect boundary, retaining its vertex coordinates, boundary topology, and local normal information, and establishing a spatial correspondence between the patch and the original artifact. As shown in Figure 6, the patch maintains geometric correspondence with the surviving artifact body but functions as an independent entity during the appearance processing stage, thereby confining the subsequent reconstruction of lighting and engraved patterns to the damaged area.

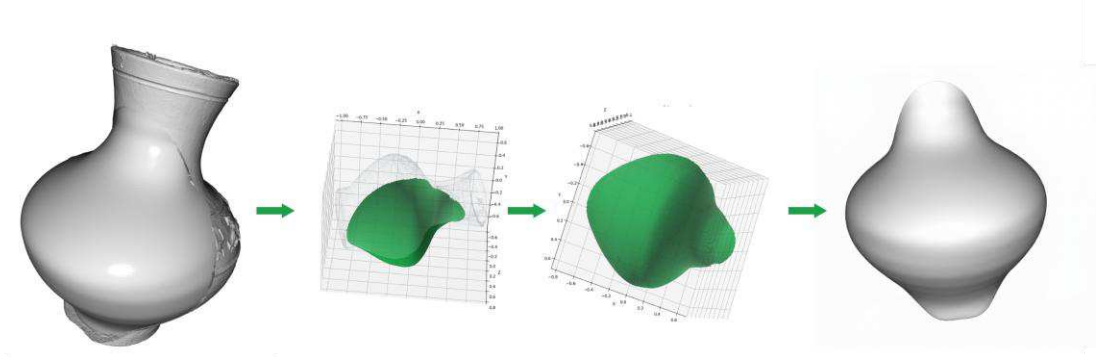

Fig. 6. Independent 3D representation of the smooth ceramic surface patch. (Source: Drawn by the author.)

For smooth ceramic surfaces, this study extracts valid tiles from a grayscale dataset lacking distinct incisions. After size normalization and grayscale normalization, a Gaussian low-pass filter is applied to decompose the observed image into low-frequency luminance components and high-frequency residuals:

$$I(x,y) = L(x,y) + R(x,y)$$
$$L(x,y) = \mathcal{G}_\sigma * I(x,y)$$

where$\big(I(x,y)\big)$ is the original grayscale image,$\big(L(x,y)\big)$ represents the low-frequency brightness component,$\big(R(x,y)\big)$ is the high-frequency residual, and$(\mathcal{G}_\sigma)$ is a Gaussian filter kernel with a standard deviation of(σ) (In the experiment, for images with a resolution of512×512 ,$\sigma = 15$ pixels were used). Given that smooth ceramic surfaces exhibit relatively continuous grayscale transitions, this paper employs Principal Component Analysis (PCA) to model the low-frequency component and extract the primary light-and-shadow variation patterns through feature decomposition. Its low-dimensional reconstruction form is:

$$\hat{L} = \boldsymbol{\mu} + \sum_{i=1}^{k} a_i \, \mathbf{u}_i$$

where$(\boldsymbol{\mu})$ is the average apparent pattern of the low-frequency samples,$(\mathbf{u}_i)$ is the (i)th principal component,(a_i) is the corresponding projection coefficient, and(k) is the number of retained principal components. The expression range of the statistical basis is determined by the cumulative explained variance, and the reconstruction mean squared error on held-out samples is used to evaluate its reconstruction performance on samples not included in the fitting. The learned low-frequency prior is used to describe the continuous light-dark variations on the ceramic surface, rather than directly restoring the material's intrinsic reflectance properties or true surface depth.

For engraved ceramic surfaces, grooves, raised ridges, and continuous decorative lines typically form directional local grayscale variations; relying solely on a low-frequency apparent model can easily weaken the edges and relief features of the patterns. Therefore, this paper extracts high-frequency residuals$\big(R(x,y)\big)$ from an independent set of engraved grayscale data and further calculates the grayscale gradient amplitude:

$$G(x,y) = \sqrt{\left(\frac{\partial I}{\partial x}\right)^2 + \left(\frac{\partial I}{\partial y}\right)^2}$$

Here, the high-frequency residuals are used to characterize the local light-dark variations in the engraved regions, while the gradient amplitude is used to highlight groove edges and decorative structures. Through feature normalization and PCA, major statistical patterns are extracted to construct an engraved surface prior that reflects the patterns' direction, spatial frequency, and local topographic lighting characteristics.

During the patch-based appearance reconstruction stage, the optimal principal component projection coefficientsa_i are first determined via a regularized least-squares fit based on the remaining surface features in the expanded neighborhood outside the defect boundary, thereby reconstructing a two-dimensional appearance feature map of the defect region. Subsequently, a conformal UV inverse mapping is used to project the two-dimensional surface prior onto an independent three-dimensional geometric patch carrier, and type-specific local modulation is performed based on boundary neighborhood information: for smooth regions, low-frequency light-and-shadow components derived from the neighborhood grayscale distribution are used to modulate the transition between light and dark in the patch's diffuse reflection; for engraved regions, high-frequency residuals and gradient features are converted into micro-surface height displacements along the patch vertex normals (normal-directed displacement modulation) based on the direction, spacing, and intensity of the remaining patterns, thereby generating a three-dimensional visual hierarchy of relief on the patch surface that seamlessly blends with the neighboring patterns. The entire appearance reconstruction process is strictly confined to the newly added geometric patches, fully preserving the geometric and appearance information of the original intact regions.

This paper primarily investigates the learning of local relief features in engraved

patterns and the generation of three-dimensional details; it does not address constraints related to pattern semantics or specific decorative content. By statistically modeling the high-frequency residuals, gradient variations, and spatial distribution patterns in grayscale images of engraved patterns, representative relief appearance priors are extracted. Combined with the surface structure of three-dimensional patches and the characteristics of neighboring patterns, these priors provide a basis for generating and reconstructing local engraved details. This method emphasizes the representation of local relief appearance and its visual continuity, achieving a harmonious balance between the geometric reconstruction of the object's main body and the reconstruction of surface engraving details.

2.4 Experimental Design and Evaluation

To evaluate the restoration performance of the proposed method under different damage conditions, this paper conducts experiments on three aspects: geometric reconstruction accuracy, surface-prior representation capability, and patch-detail continuity. Geometric evaluation uses the complete scan model as the ground truth, focusing on the damaged areas and their boundary transition zones to avoid the influence of undamaged areas on the overall error. , Chamfer Distance (CD), 95% Hausdorff Distance (HD95), Normal Consistency (NC), and cross-sectional contour error were used to evaluate the quality of geometric completion. Among these, CD is used to measure the bidirectional average spatial distance between the generated patch and the corresponding region of the reference model, defined as:

$$\mathrm{CD}(P,Q)=\frac{1}{2}\left(\frac{1}{|P|}\sum_{p\in P}\min_{q\in Q}\|p-q\|_2+\frac{1}{|Q|}\sum_{q\in Q}\min_{p\in P}\|q-p\|_2\right)$$

where(P) and(Q) represent the sets of sample points for the reconstructed patch and the corresponding defect region of the complete reference model, respectively. HD95 is used to evaluate larger local geometric deviations; NC measures the consistency between the reconstructed and reference surfaces; and cross-sectional contour error is used to assess the accuracy of radial contour reconstruction of the inner and outer walls. All distance metrics are calculated at a unified model scale.

Surface prior evaluation employs the Mean Squared Error (MSE) of the reconstruction and the cumulative variance explained by PCA. For smooth ceramics, the results of retaining low-frequency light and dark components from the sample are compared with the PCA reconstruction results; for engraved ceramics, the statistical reconstruction errors of high-frequency residuals and grayscale gradient features are evaluated. MSE is defined as:

$$\mathrm{MSE}=\frac{1}{N}\sum_{i=1}^{N}\left(f_i-\hat{f}_i\right)^2$$

where(f_i) and$\left(\hat{f}_i\right)$ represent the target features and reconstructed values, respectively, and(N) is the number of valid features. MSE and the cumulative variance explained by PCA are used to evaluate the statistical basis's ability to represent target features: for smooth ceramics, this evaluates the reconstruction performance of low-frequency light-dark

components; for incised ceramics, it evaluates the reconstruction performance of high-frequency residuals and grayscale gradient features. The 3D patch application, meanwhile, uses visual analysis to examine overall light-dark transitions, the direction of local engravings, and the fit near defect boundaries.

The geometric experiments used samples with four levels of artificial defects (15%, 30%, 45%, and 60%) and combined geometric error analysis with graphical morphological interpretation to analyze reconstruction performance under different defect configurations. In the surface statistics experiments, we compared the training and validation reconstruction results for the smooth prior with 8 and 16 principal components, as well as for the engraved prior with 8, 16, and 24 principal components. Subsequently, we applied the priors to independent 3D patches to demonstrate their performance in continuous shading expression and in generating local engraved details. The above evaluations correspond to geometric accuracy, statistical expression capability, and surface application effectiveness, respectively; the main evaluation criteria are shown in Table 1.

Table 1. Evaluation metrics for ceramic digital restoration.

Evaluation Object	**Evaluation Metrics**	**Evaluation Content**	**Nature and Criteria of Evaluation**
Geometric Restorations	CD	Average Spatial Deviation	Quantitative (Lower is better)
Geometric Restorations	HD95	Large Local Geometric Deviation	Quantitative (Lower is better)
Surface Structure	NC	Surface Normal Consistency	Quantitative (Higher is better)
Tool Profile	Radial Cross-Section Error	Inner and Outer Wall Contour Recovery Accuracy	Quantitative (Lower is better)
Light and Shadow and Engraving Prior	MSE	Grayscale and Feature Reconstruction Error	Quantitative (Lower is better)
Apparent statistical model	Cumulative Variance Explained by PCA	Expressive Power of Major Apparent Patterns	Quantitative (Higher is better)
Patch Surface	Surface Visualization Analysis	Visual and Geometric Continuity	Qualitative (Qualitative assessment)

3. Results

This chapter validates the proposed two-stage digital restoration method in three aspects: 3D geometric reconstruction, reconstruction of surface lighting and shadows, and generation of engraved relief details. First, we analyze the geometric restoration results for different artifact types and damage severity levels. Next, we evaluate the statistical

reconstruction capabilities of lighting and engraved-relief priors, as well as their performance on 3D restoration patches. Finally, we compare the actual performance of each stage using multidimensional quantitative metrics and parameters.

3.1 Geometric Reconstruction Results

To analyze the performance of the geometric constraint method under different damage conditions, this paper focuses on the spatial coverage of the generated patches, the preservation of the artifact's contour, and the continuity of adjacent surfaces. Figure 7 shows the geometric restoration results for three representative artifacts under different damage levels, along with their corresponding projected contours.

In the figure, orange represents the original surviving surface, while gray represents the geometrically reconstructed patch; these colors are used solely to distinguish the observation area from the reconstruction area and do not represent the final glaze color or surface texture. The curves on the far right represent the projected half-width contour extracted from the rendered images of the artifacts and their smoothed result, respectively, which are used to assist in analyzing the main contour features of the vessel shape.

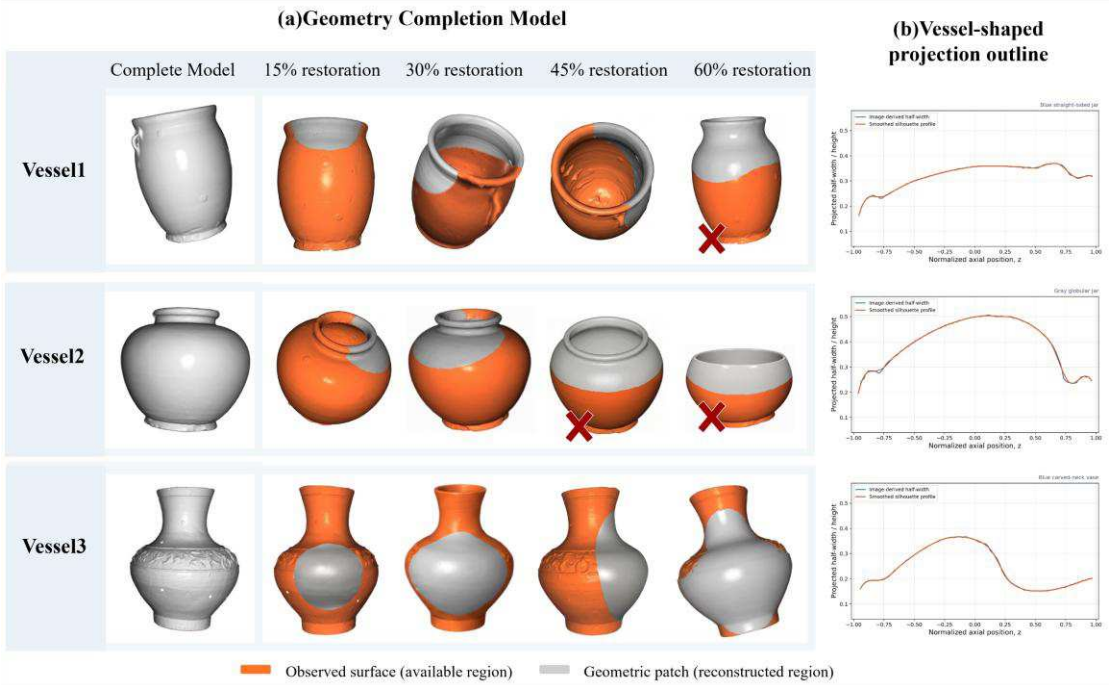

Fig. 7. Completion Results for Different Defect Geometries. (a) Geometry Completion Model; (b) Vessel-shaped projection outline (Source: Drawn by the author.)

As shown in Figure 7, there are significant differences in the effectiveness of geometric reconstruction across different vessel types and degrees of damage. The primary factors influencing this outcome include not only the area of damage but also the extent to which key structural information is preserved. For Vessel 1 and Vessel 2, at lower damage ratios, the remaining rim and adjacent vessel walls provide effective constraints on the cross-sectional contour, allowing the generated patches to largely preserve the vessel body's overall shape. However, when the loss ratio for Object 1 increased to 60%, and for Object 2 to 45% and 60%, the rim structure was completely lost. This prevented the intact cross-section at the

corresponding height from providing a reliable radial reference, resulting in significant deviations from the original shape in the reconstruction and failing to meet the requirements for geometric restoration. In contrast, although Object 3 lost most of its body surface under 60% damage, the rim and some key contours remained intact; consequently, the patch was still able to reconstruct the main surface from the remaining structure, demonstrating good form continuity.

To further quantify the geometric restoration effectiveness of the patches, the reconstructed patches were compared with the complete reference models; the results are summarized in Table 2. The evaluation was limited to the actual damage areas to avoid the influence of intact regions on error statistics. Among these, the cases involving Object 1 (60% loss) and Object 2 (45% and 60% loss) did not meet the requirements for effective reconstruction due to the complete loss of key rim structures. Table 2 presents the average geometric errors for all three test objects across various loss percentages and simultaneously lists the morphological interpretation pass rates to determine the method's applicability limits under conditions of severe structural information loss by combining quantitative deviations with qualitative morphological analysis.

Table 2. Quantitative Evaluation of Geometric Completion (Lower values for CD, HD95, and radial cross-sectional error are better; higher values for NC are better)

Defect Ratio	Number of Effectively Reconstructed Artifacts	CD	HD95	NC	Radial Deviation of Cross-Section ↓
15%	3/3	0.0068	0.0195	0.965	0.0081
30%	3/3	0.0109	0.0327	0.941	0.0136
45%	2/3	0.0178	0.0523	0.909	0.0234
60%	1/3	0.0265	0.0812	0.871	0.0359

Note: Three artifacts were tested for each defect ratio. "Valid Reconstruction" was qualitatively assessed based on the preservation of the main contour shown in Figure 7 and the alignment of the patch with. This indicates that the generated patch covers the main defect area and forms a generally reasonable overall shape relative to the remaining artifact; cases exhibiting obvious distortion of the rim shape or deviation from the main artifact form were classified as failures. This classification is used to distinguish the morphological usability of the current cases and does not replace evaluations of geometric accuracy. CD, HD95, and radial cross-sectional error are all expressed on a unified model scale; NC is used to describe the normal consistency between the reconstructed and reference surfaces; the number of "effective completions" and geometric error metrics reflect the morphological assessment results and spatial deviations of the cases, respectively.

Combining Figure 7 and Table 2, the method demonstrates good overall morphological continuity when key contour information is sufficiently preserved, whereas cases with high levels of damage—such as those with the rim entirely missing—exhibit significant deviations in vessel shape. Vessel 3 retains its main contour even with 60% damage, suggesting that the proportion of damaged area alone is insufficient to characterize the difficulty of restoration in

a given case; the preservation status of the rim and key cross-sections should also be analyzed in conjunction. These results reflect the method's varying applicability across the test artifacts and damage configurations examined in this paper, and illustrate that, when evaluating reconstruction results, attention must be paid to both the scale of the damage and the morphological evidence provided by the surviving structure.

3.2 Light and Shadow Reconstruction on Smooth Surfaces

To evaluate the statistical representation and reconstruction capabilities of prior knowledge regarding light and shadow on smooth ceramic surfaces, this study conducted low-frequency apparent learning based on preprocessed grayscale data and validated the results using independently set-aside samples and 3D surface applications. Figure 8 displays a typical smooth ceramic grayscale sample, the low-frequency light-and-shadow reconstruction results, samples generated from statistical prior knowledge, and the 3D surface visualization.

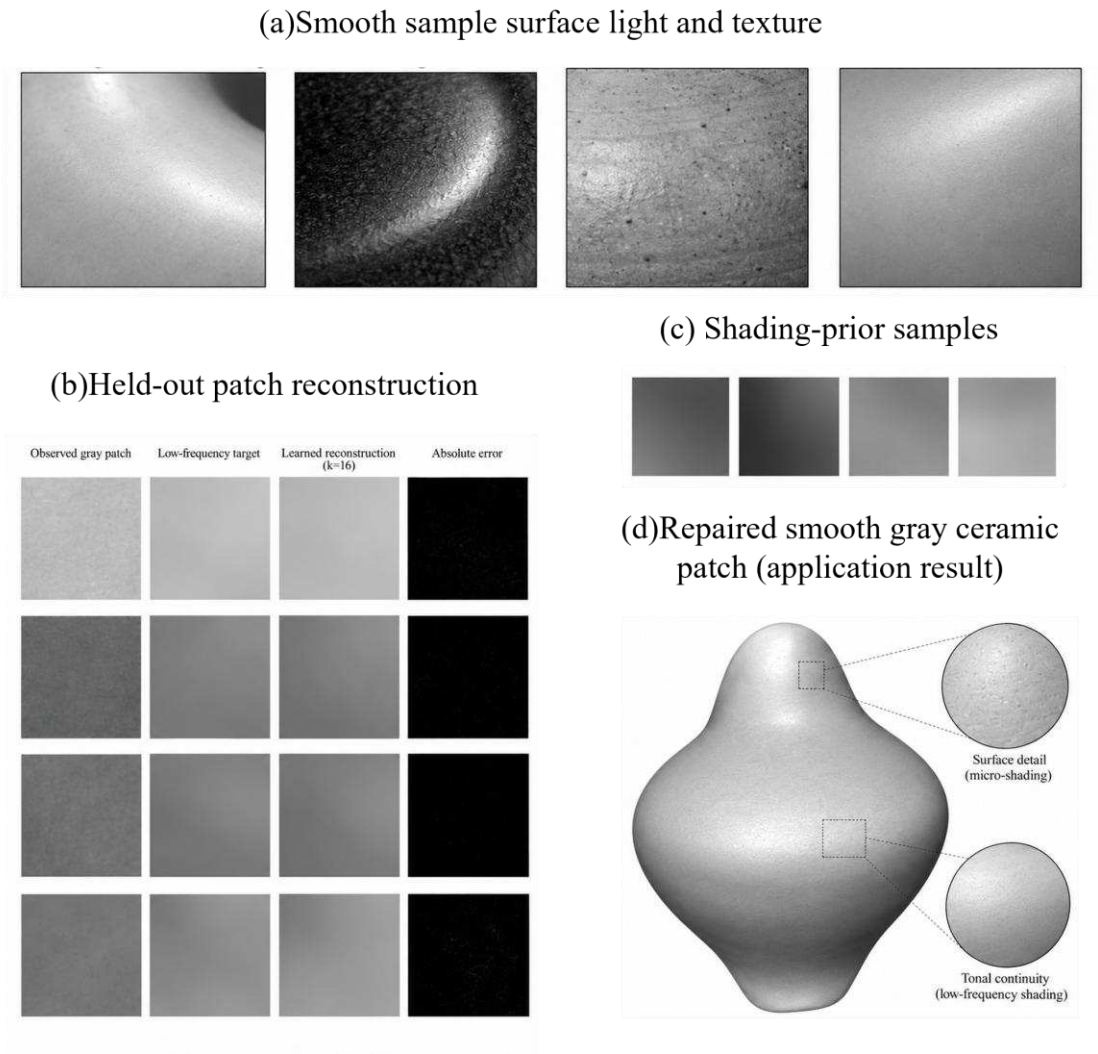

Fig. 8 Validation of the learning and reconstruction of grayscale appearance priors for smooth ceramic surfaces. (a) Grayscale samples of smooth surfaces; (b) Reconstruction results for held-out patches; (c) Sampled shading priors; (d) 3D patch application and local surface details. (Source: Drawn by the author.)

As shown in Figure 8(a), smooth ceramic samples differ in overall brightness, grayscale gradients, and local fine-grained features. Low-frequency decomposition suppresses local high-frequency variations and preserves a continuous distribution of light and dark across a broader range. Figure 8(b) presents four sets of reconstruction examples for held-out samples, illustrating the relationship between low-frequency targets, PCA reconstruction, and absolute error. Table 3 reports statistical results for different numbers of principal components, showing that the held-out MSE for the smooth prior is 0.0035 when 16 principal components are retained. The illustrated results, together with statistical metrics, are used to evaluate the expressive power of low-dimensional statistical bases for continuous light-dark variations.

Figure 8(c) further illustrates light-and-shadow prior samples extracted from the learned statistical space. The different samples exhibit variations in brightness levels, gradient directions, and the amplitude of change, while maintaining continuous, smooth transitions between light and dark, reflecting the statistical model's ability to represent the diversity of light-and-shadow distributions on ceramic surfaces. These light and shadow patterns can serve as candidate priors for coordinating light and shadow within patches across different curvatures and local surface conditions, enabling the generated regions to exhibit corresponding light and shadow variations based on neighborhood grayscale features.

To further examine the performance of the lighting priors on 3D surfaces, Figure 8(d) shows the results of lighting reconstruction and local detail visualization on a smooth ceramic surface. The overall surface exhibits continuous gradations of light and dark, reflecting the light-and-shadow distribution produced by changes in the object's curvature; the locally magnified areas reveal subtle grayscale variations and surface light-dark gradations. By coordinating low-frequency light-and-shadow distribution with local microscopic appearance, the reconstructed surface exhibits relatively natural details while maintaining the continuity of the overall tonal quality, thereby providing a basis for the visual reconstruction of geometric patches.

3.3 Detail Reconstruction of Engraved Surfaces

To evaluate the feature representation and detail-generation capabilities of the prior model for the relief appearance of incised surfaces, this study conducted high-frequency feature analysis and statistical reconstruction using grayscale samples of incised ceramics, and examined the generation of local relief details in conjunction with 3D patches. Figure 9 ( ) illustrates a typical incised sample, relief feature extraction, PCA statistical patterns, reconstruction error variations, and application results on patch surfaces.

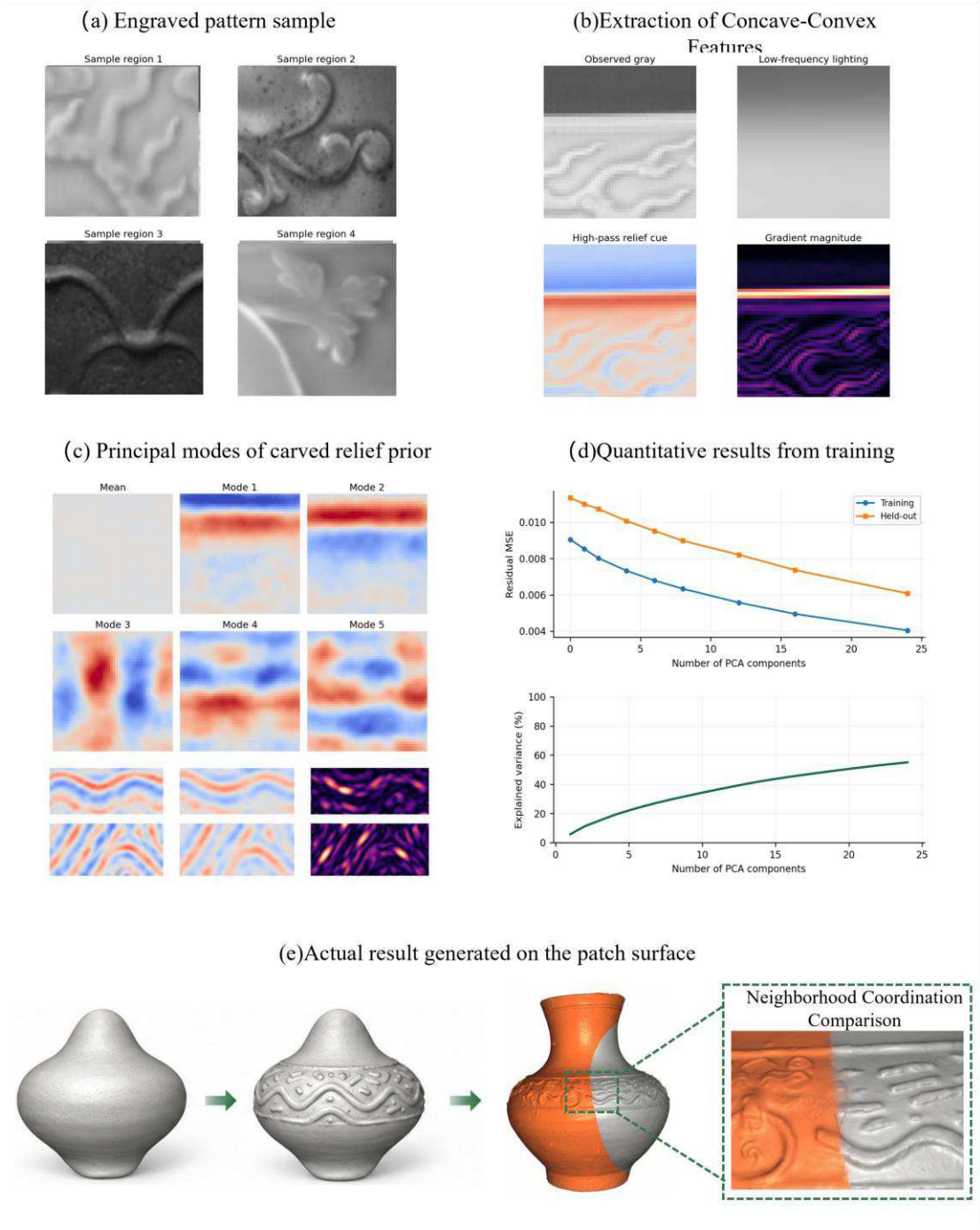

Figure 9. Extraction and reconstruction validation of relief appearance priors for carved ceramic surfaces. (a) Engraved sample; (b) Multi-scale bump clues; (c) PCA prior; (d) Training and hold-out results; (e) Application on patch surface. (Source: Drawn by the author.)

As shown in Figure 9(a), different carved samples exhibit significant differences in decorative patterns, groove widths, and local variations in brightness and darkness. Figure 9(b) illustrates the feature decomposition results of the engraved areas. After low-frequency brightness separation, the high-frequency residuals retain the grayscale variations on both sides of the grooves and ridges, while the gradient amplitude further highlights the edges and

linear structures of the patterns. These two types of features collectively characterize the local intensity and spatial distribution of the engraved patterns, providing a foundation for subsequent statistical prior learning.

Figure 9(c) displays the average pattern of the engraved features and the top five PCA principal components. Different modes exhibit features such as stripes, ripples, and local positive and negative responses, reflecting differences in the spatial frequency, orientation, and relief distribution of the engraved patterns. Among these, lower-order modes primarily describe grayscale variations over larger areas, while higher-order modes supplement the detailed characteristics of local patterns. By combining different statistical modes, candidate prior models for engraved patterns with diverse local relief patterns can be constructed.

Figure 9(d) and Table 3 report the feature reconstruction error and cumulative explained variance for different numbers of principal components. Within the range of principal components tested in this study, increasing the number of principal components reduces the reconstruction error of the defined features. This result is used to evaluate the expressive power of the PCA statistical basis; however, its explanatory scope is limited to the current features, data partitioning, and preprocessing conditions. Since the smoothing prior and the engraved prior target different features, the MSE and cumulative explained variance for these two types of priors cannot be used directly as a basis for a side-by-side comparison of restoration quality. For the low-frequency light-and-shadow patterns of smooth ceramics, the cumulative explained variance was 93.60% when 16 principal components were retained, with a holdout-set MSE of 0.0035; the engraved prior further examined the statistical reconstruction performance with 24 principal components.

Table 3. Statistical reconstruction performance of ceramic appearance priors with different numbers of PCA components.

Prior Type	**Number of PCA Components**	**Training Set MSE ↓**	**Validation Set MSE ↓**	**Cumulative Explained Variance (%) ↑**
Smooth Ceramic Low-Frequency Light and Shadow	8	0.0051	0.0068	84.20
Smooth Ceramic Low-Frequency Light and Shadow	16	0.0028	0.0035	93.60
Engraved Ceramic with Textured Surface	8	0.0063	0.0090	31.50
Apparent Surface Roughness of Engraved Ceramics	16	0.0049	0.0074	45.80

Apparent Surface Roughness of Engraved Ceramics	24	0.0040	0.0061	55.40

Figure 9(e) shows the results of applying the engraved pattern appearance prior to the patch. Under the rendering conditions shown, the patch with the prior applied exhibits visual depth in the grooves and raised ridges. A close-up view is provided to observe the orientation and tonal transitions between the generated areas and the remaining decoration near the boundaries. This demonstration constitutes qualitative visual evidence; it is not sufficient on its own to assess the accuracy of the reconstruction of the actual incised depth, nor can it confirm that the generated patterns match the original historical ones.

Based on the above results, the high-frequency residuals and gradient features of engraved ceramics can effectively characterize the local topographical variations of the patterns, while the PCA statistical prior provides a feature-based foundation for combining and generating different undulation patterns. By integrating 3D patches with neighboring pattern information, it is possible to further generate and visually harmonize local engraved details, which, together with low-frequency lighting and shadow reconstruction, form a classification-based restoration system tailored to different surface characteristics.

4. Discussion

This study demonstrates that integrating geometric structure and surface appearance priors for ceramic artifacts can effectively support the restoration of overall form and the reconstruction of local details in damaged artifacts. Under the condition that key structural information is preserved, the reconstruction results effectively maintain the main body's form and cross-sectional continuity, consistent with the conclusions of previous studies. Xu et al. employed a multiscale diffusion strategy to fill in missing parts of the Terracotta Army [3], while Wu et al. improved point cloud completion results by incorporating explicit structural priors [10]; both studies confirmed the crucial role of structural information in 3D form restoration. In contrast, this paper introduces the primary defect boundary, the contour of the intact cross-section, and local symmetry credibility without altering the core structure of the pre-trained AdaPoinTr model, thereby imposing the artifact's own geometric constraints on the generated patches. The current case study demonstrates that when analyzing restoration results, it is necessary to simultaneously consider the proportion of the defect, its location, and the preservation status of key contours. When key structures, such as the rim, are missing, the local contour constraints provided by the artifact are reduced, and the reconstruction results may deviate from the original form. Furthermore, the low-frequency light-and-shadow patterns on smooth, glazed surfaces and the high-frequency relief features in incised areas exhibit different levels of statistical complexity, indicating that type-based surface priors help coordinate form restoration with local detail reconstruction, thereby further expanding the application of structural priors in the digital restoration of ceramics.

This study provides a practical technical approach for the digital restoration of ancient ceramics. The generated 3D geometric patches can serve as a reference for morphological inference and the design of restoration plans in traditional restoration. After geometric

verification and expert evaluation, these patches can be combined with 3D printing technology to produce physical restoration components, which help determine the shape of the patches and their connection to the original vessel wall [33]. At the same time, the reconstruction of light and shadow on smooth surfaces and the relief details of incised patterns can enhance the visual integrity of digital models, supporting museum digital exhibitions, virtual restoration, and the development of digital archives for cultural relics [34]. By combining the original scan model with 3D rendering technology, conservators can also compare the forms and surface effects of different restoration proposals. Compared with simple two-dimensional texture restoration, this study employs 3D geometric patches as the basis for surface detail reconstruction, thereby achieving spatial correspondence between the artifact's form and its visual characteristics and providing a technical reference for bridging physical restoration and digital preservation.

Although this study has made some progress, certain unavoidable limitations remain. First, the reconstruction of engraved patterns primarily relies on grayscale gradients, high-frequency residuals, and statistical priors to simulate the local relief and light-and-shadow variations of the decorative motifs. It has not yet achieved accurate restoration of the original patterns' semantics, specific decorative themes, or historical compositions; therefore, the generated results cannot be directly equated with a true restoration of the historical decorative patterns [35]. Second, geometric reconstruction relies heavily on key structural information. When extensive damage results in the complete loss of the rim, making it impossible to determine the original rim diameter and related cross-sectional information, local constraints cannot provide sufficient morphological evidence, and the reconstruction results will rely more heavily on the overall shape priors learned by the model. In such cases, even if the generated patches exhibit visual continuity, they may deviate from the artifact's true form; some cases with a high proportion of damage have already exhibited significant deviations in vessel shape. Furthermore, this study was validated using only three nearly axially symmetric ceramic artifacts, with damage conditions primarily constructed artificially. The sample set has limited coverage in terms of vessel forms, materials, and decorative styles, which is insufficient to demonstrate the method's general applicability to complex, irregularly shaped artifacts and real-world irregular damage.

In summary, the two-stage restoration method proposed in this paper—combining geometric constraints with surface prior information—effectively integrates the reconstruction of the ceramic's primary form with the restoration of surface lighting, shadows, and the relief details of incised patterns. The present study provides case references for patch construction and typological surface representation of nearly axisymmetric ceramic objects. Future research could incorporate ceramic form classification, archaeological typological knowledge, and structural references from intact objects of the same type to enhance the ability to infer form under conditions of complete loss in key areas; by integrating historical ceramic color patterns [36], multi-view color textures, 3D surface normals, and high-precision engraving depth information, we will explore collaborative reconstruction methods that account for both the semantic meaning of patterns, the topographical geometry, and material shading; simultaneously, we will expand the dataset to include different artifact categories and authentic damage samples, combining quantitative

geometric evaluation with assessments by cultural heritage restoration experts to further validate the method's reconstruction accuracy, stability, and scope of application. This study provides an interpretable digital restoration approach for ancient ceramics, ranging from macro-level morphological recovery to the reconstruction of local surface details.

Data Availability

The datasets generated and analyzed during the current study are available from the corresponding author upon reasonable request.

References

[1] NÚÑEZ-ANDRÉS M A, BUILL F, DE MESA A. Virtual reconstruction of archaeological pottery using visual programming language[J]. Journal of Archaeological Science: Reports, 2024, 56: 104533. DOI: 10.1016/j.jasrep.2024.104533.

[2] LAMB N, PALMER C, MOLLOY B, et al. Fantastic Breaks: A dataset of paired 3D scans of real-world broken objects and their complete counterparts[C]// Proceedings of the IEEE/CVF Conference on Computer Vision and Pattern Recognition. 2023: 4681–4691.

[3] XU X, SONG D, GENG G, et al. CPDC-MFNet: Conditional point diffusion completion network with Muti-scale Feedback Refine for 3D Terracotta Warriors[J]. Scientific Reports, 2024, 14: 8307. DOI: 10.1038/s41598-024-58956-1.

[4] YU X, RAO Y, WANG Z, et al. AdaPoinTr: Diverse point cloud completion with adaptive geometry-aware transformers[J]. IEEE Transactions on Pattern Analysis and Machine Intelligence, 2023, 45(12): 14114–14130. DOI: 10.1109/TPAMI.2023.3309253.

[5] LI S, GAO P, TAN X, WEI M. ProxyFormer: Proxy alignment assisted point cloud completion with missing part sensitive transformer[C]// Proceedings of the IEEE/CVF Conference on Computer Vision and Pattern Recognition. 2023: 9466–9475.

[6] CHEN Z, LONG F, QIU Z, et al. AnchorFormer: Point cloud completion from discriminative nodes[C]// Proceedings of the IEEE/CVF Conference on Computer Vision and Pattern Recognition. 2023: 13581–13590.

[7] WANG J, CUI Y, GUO D, et al. PointAttN: You only need attention for point cloud completion[C]// Proceedings of the AAAI Conference on Artificial Intelligence. 2024, 38(6): 5472–5480. DOI: 10.1609/aaai.v38i6.28356.

[8] KASTEN Y, RAHAMIM O, CHECHIK G. Point cloud completion with pretrained text-to-image diffusion models[C]// Advances in Neural Information Processing Systems. 2023, 36: 12171–12191.

[9] LI Y, ZHOU Q, GONG J, et al. DAPoinTr: Domain adaptive point transformer for point cloud completion[C]// Proceedings of the AAAI Conference on Artificial Intelligence. 2025, 39(5): 5066–5074. DOI: 10.1609/aaai.v39i5.32537.

[10] WU Z, SHI J, DENG X, et al. SPAC-Net: Rethinking point cloud completion with structural prior[J]. IEEE Transactions on Visualization and Computer Graphics, 2025, 31(9): 6268–6279. DOI: 10.1109/TVCG.2024.3507013.

[11] WANG Z R, LIU X D, ZHOU M Q. 3D model hole filling in cultural relics' facial reconstruction fusion diffusion model[J]. Journal of Northwest University (Natural Science Edition), 2025, 55(1): 213–222. DOI: 10.16152/j.cnki.xdxbzr.2025-01-018. (in Chinese).

[12] ZHANG X. AI-assisted restoration of Yangshao painted pottery using LoRA and Stable

Diffusion[J]. Heritage, 2024, 7(11): 6282–6309. DOI: 10.3390/heritage7110295.

[13] KANG X, YANG G. Intelligent restoration expert system design for Jingdezhen export porcelain via improved denoising diffusion probabilistic model[J]. npj Heritage Science, 2025, 13: 297. DOI: 10.1038/s40494-025-01890-w.

[14] LIAO D, ZENG T, YANG J, et al. Digital prediction of ancient ceramic images missing areas based on deep adversarial and reverse diffusion[J]. npj Heritage Science, 2025, 13: 242. DOI: 10.1038/s40494-025-01797-6.

[15] ZHANG L, RAO A, AGRAWALA M. Adding conditional control to text-to-image diffusion models[C]// Proceedings of the IEEE/CVF International Conference on Computer Vision. 2023: 3836–3847. DOI: 10.1109/ICCV51070.2023.00355.

[16] KUMARI N, ZHANG B, ZHANG R, et al. Multi-concept customization of text-to-image diffusion[C]// Proceedings of the IEEE/CVF Conference on Computer Vision and Pattern Recognition. 2023: 1931–1941. DOI: 10.1109/CVPR52729.2023.00192.

[17] JU X, LIU X, WANG X, et al. BrushNet: A plug-and-play image inpainting model with decomposed dual-branch diffusion[C]// Computer Vision – ECCV 2024. Lecture Notes in Computer Science, 2024, 15078: 150–168. DOI: 10.1007/978-3-031-72661-3_9.

[18] ZHUANG J, ZENG Y, LIU W, et al. A task is worth one word: Learning with task prompts for high-quality versatile image inpainting[C]// Computer Vision – ECCV 2024. Lecture Notes in Computer Science, 2024, 15116: 195–211. DOI: 10.1007/978-3-031-73636-0_12.

[19] WU M, GUO G, SUN Z G, et al. Tomb mural inpainting with adaptive convolutional constraints and global context inference[J]. Journal of Image and Graphics, 2025, 30(3): 737–754. DOI: 10.11834/jig.240277. (in Chinese).

[20] HU J, YU Y, ZHOU Q. GuidePaint: Lossless image-guided diffusion model for ancient mural image restoration[J]. npj Heritage Science, 2025, 13: 118. DOI: 10.1038/s40494-025-01693-z.

[21] LI Y, ZHANG C, LI Y, et al. An improved mural image restoration method based on diffusion model[J]. npj Heritage Science, 2025, 13: 347. DOI: 10.1038/s40494-025-01914-5.

[22] DING Y, WU K, TIAN B. Frequency-domain information guidance: Diffusion models for the inpainting of Dunhuang murals[J]. Knowledge-Based Systems, 2025, 314: 113188. DOI: 10.1016/j.knosys.2025.113188.

[23] TIAN B, ZHOU Y L, SHAN H Q, et al. HASM: Restoration of Dunhuang murals with spatial structure prediction and line drawing assisted guidance[J]. Journal of University of Electronic Science and Technology of China, 2025, 54(4): 582–591. DOI: 10.12178/1001-0548.2024241. (in Chinese).

[24] REN Y, LU H, LIU C. Kraak porcelain decorative pattern restoration using generative AI: A pilot study[J]. Scientific Reports, 2025, 15: 36347. DOI: 10.1038/s41598-025-20180-w.

[25] CAO T, KREIS K, FIDLER S, et al. TexFusion: Synthesizing 3D textures with text-guided image diffusion models[C]// Proceedings of the IEEE/CVF International Conference on Computer Vision. 2023: 4169–4181. DOI: 10.1109/ICCV51070.2023.00385.

[26] ZENG X, CHEN X, QI Z, et al. Paint3D: Paint anything 3D with lighting-less texture diffusion models[C]// Proceedings of the IEEE/CVF Conference on Computer Vision and Pattern Recognition. 2024: 4252–4262.

[27] PATHAK S, KUMAR P, BAIJU D, et al. Revisiting point cloud completion: Are we ready for the real-world?[C]// Proceedings of the IEEE/CVF International Conference on Computer Vision. 2025: 25388–25398.

[28] LI J, PENG C, GU W, et al. A point cloud simplification method using clustering and saliency for cultural heritage reconstruction[J]. npj Heritage Science, 2025, 13: 445. DOI: 10.1038/s40494-025-02016-y.

[29] HU C, XIE Y, XIA G, et al. An automatic annotation method for colored 3D triangular meshes oriented to cultural relic deterioration segmentation[J]. npj Heritage Science, 2026, 14: 150. DOI: 10.1038/s40494-026-02421-x.

[30] WU Y, YAN Z, CHEN C, et al. SCoDA: Domain adaptive shape completion for real scans[C]// Proceedings of the IEEE/CVF Conference on Computer Vision and Pattern Recognition. 2023: 17630–17641.

[31] ZHENG Q, YANG H, YANG J, et al. Ancient ceramics restoration method based on image processing texture stitching[J]. Heritage Science, 2024, 12: 423. DOI: 10.1186/s40494-024-01539-0.

[32] COUPRY B, BRUMENT B, LAURENT A, et al. Assessing the quality of 3D reconstruction in the absence of ground truth: Application to a multimodal archaeological dataset[C]// Proceedings of the IEEE/CVF Winter Conference on Applications of Computer Vision. 2025: 3457–3466. DOI: 10.1109/WACV61041.2025.00341.

[33] BISHOP S U, ARSHAD M, LAZOĞLU I, et al. Photogrammetry, additive manufacturing, and sensorization for archaeological ceramic loss compensation[J]. Journal of Cultural Heritage, 2025, 76: 148–156. DOI: 10.1016/j.culher.2025.09.012.

[34] FURFERI R, DI ANGELO L, BERTINI M, et al. Enhancing traditional museum fruition: Current state and emerging tendencies[J]. Heritage Science, 2024, 12: 20. DOI: 10.1186/s40494-024-01139-y.

[35] XU J, YAN L, ZHANG R, et al. A review of the development and application of generative technology in digital museums[J]. npj Heritage Science, 2025, 13: 589. DOI: 10.1038/s40494-025-02164-1.

[36] WANG Y, SI Z, WANG W, et al. Uncovering historical ceramic color patterns via visual analytics for design and heritage[J]. npj Heritage Science, 2026, 14: 77. DOI: 10.1038/s40494-026-02314-z.

Acknowledgments

Project:

This work was supported by the Innovation Capacity Support Program of Shaanxi Province (Project No. 2025JC-GXPT-007).

Author contributions

Y.W.: Conceptualization, Supervision, Writing—Review.
Z.S.: Methodology, Visualization, Writing—Original Draft.

J.Z.: Validation.

T.W.: Validation.

M.Q.: Validation.

Y.Z. Validation.
W.W.: Supervision.
J.C.: Supervision.
X.Y.: Supervision.
All authors reviewed the manuscript.

Conflicts of Interest

The authors declare no competing interests.